

Accepted Manuscript

Synthesis, X-ray structure, theoretical investigation, corrosion inhibition and antimicrobial activity of benzimidazole thioether and their metal complexes

Mehdi Bouchouit, Said Mohamed Elhadi, Mounira Kara Ali, Sofiane Bouacida, Hocine Merazig, Nourreddine Kacem Chaouche, Aissa Chibani, Bachir Zouchoune, Ali Belfaitah, Abdelmalek Bouraiou

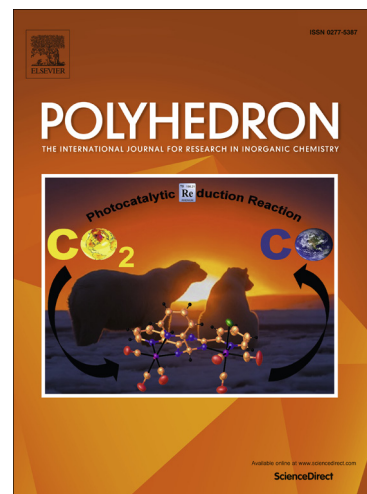
PII: S0277-5387(16)30414-4
DOI: <http://dx.doi.org/10.1016/j.poly.2016.08.045>
Reference: POLY 12182

To appear in: *Polyhedron*

Received Date: 28 June 2016
Revised Date: 21 August 2016
Accepted Date: 24 August 2016

Please cite this article as: M. Bouchouit, S. Mohamed Elhadi, M. Kara Ali, S. Bouacida, H. Merazig, N. Kacem Chaouche, A. Chibani, B. Zouchoune, A. Belfaitah, A. Bouraiou, Synthesis, X-ray structure, theoretical investigation, corrosion inhibition and antimicrobial activity of benzimidazole thioether and their metal complexes, *Polyhedron* (2016), doi: <http://dx.doi.org/10.1016/j.poly.2016.08.045>

This is a PDF file of an unedited manuscript that has been accepted for publication. As a service to our customers we are providing this early version of the manuscript. The manuscript will undergo copyediting, typesetting, and review of the resulting proof before it is published in its final form. Please note that during the production process errors may be discovered which could affect the content, and all legal disclaimers that apply to the journal pertain.



Synthesis, X-ray structure, theoretical investigation, corrosion inhibition and antimicrobial activity of benzimidazole thioether and their metal complexes

Mehdi Bouchouit,^a Said Mohamed Elhadi,^a Mounira Kara Ali,^b Sofiane Bouacida,^{a, c} Hocine Merazig,^a Nourreddine Kacem Chaouche,^b Aissa Chibani,^a Bachir Zouchoune,^{a, c} Ali Belfaitah,^d and Abdelmalek Bouraiou^{a*}

^a Unité de Recherche de Chimie de l'Environnement et Moléculaire Structurale, Université des Frères Mentouri, Constantine 25000, Algérie

^b Laboratoire de Mycologie, de Biotechnologie et de l'Activité Microbienne, Université des Frères Mentouri, Constantine 25000, Algérie

^c Département des sciences de la matière, Université Oum El Bouaghi, 04000 Oum El Bouaghi, Algérie

^d Laboratoire des Produits Naturels d'Origine Végétale et de Synthèse Organique, Université des Frères Mentouri, Constantine 25000, Algérie

Correspondence (A. Bouraiou): bouraiou.abdelmalek@yahoo.fr; Tel.: +213-05-51-599-889; Fax: +213-031-903-558

Keywords

Benzimidazole complexes; X-Ray determination structure; Corrosion inhibition; Antimicrobial activity; Electronic structure.

Abstract

Synthesis, characterization, corrosion inhibition as well as antimicrobial activity of the coordination compounds $\{\text{Co}(\text{bbms})\text{Cl}_2\}$, $\{\text{Zn}(\text{bbms})\text{Cl}_2\}$, $\{\text{Co}(\text{btmb})\text{Cl}_2\}$ and $\{\text{Zn}(\text{btmb})\text{Cl}_2\}$ containing benzimidazole thioether have been described. $\text{Co}(\text{bbms})$ and $\text{Zn}(\text{bbms})$ as well as $\text{Co}(\text{btmb})$ and $\text{Zn}(\text{btmb})$ are isostructural with space group Pbca and P21 respectively.

The coordination polyhedron around the metal center for all complexes may be described as a quasi-regular tetragonal geometry. The corrosion inhibition study of these complexes for steel in 0.5 M H_2SO_4 medium has been investigated using potentiodynamic polarization and EIS techniques. These later show the corrosion inhibition ability of the prepared complexes for steel in acid medium. A new procedure has been developed for antimicrobial assay using a solid tablet of the corresponding complexes. These later show moderate to significant

antimicrobial activities against: *Pseudomonas syringae*, *Staphylococcus aureus* and *Pichia caribbica*. DFT/BP86 calculations have been carried out on the neutral complexes and on the monoanionic of (1) and (3) forms of singlet and triplet species. The optimized structures reproduce those observed experimentally, while the reduced ones undergo remarkable geometrical parameters.

Introduction

Benzimidazole derivatives are reported to be physiologically and pharmacologically active and have shown different biological activities such as antioxidant [1], antifungal [2], antihelmintic [3], antitumoral [4], anti-inflammatory [5] and antimicrobial [6,7]. Furthermore, benzimidazole derivatives can be also used as epoxy resin curing agents, catalysts, and metallic surface treatment agents [8,9].

The ability of benzimidazole derivatives to form stable complexes with metal ions, had given a place to a variety of metal-ligand coordination modes. Their reactions with metal salts have played a significant role in the development of coordination chemistry [11-12]. Several research teams have examined the coordination behavior of benzimidazole derivatives towards transition metal ions [13,14] and others studies have explored the biological activity of coordination compounds containing benzimidazole entity [15-17].

In other hand, benzimidazole derivatives are effective corrosion inhibitors for many metals. The efficiency of these heterocyclic derivatives is due to the presence of high-electron-density zone. These molecules types form an adsorbed protective film on the metal surface, which leads to isolating the metal surface from the corrosive environment [18-20].

In this study, we report the synthesis of four benzazole thioether metal complex namely {Co(bbms)Cl₂} (1), {Zn(bbms)Cl₂} (2), {Co(btmb)Cl₂} (3) and {Zn(btmb)Cl₂} (4) and their application for the first time as corrosion inhibitors on mild steel in 0.5 M H₂SO₄. The crystal structures of all compounds are extensively discussed and their corrosion inhibition activities are examined using electrochemical impedance spectroscopy (EIS) and Tafel polarization. The antimicrobial activities of the prepared compounds will be also evaluated.

In addition, in this study we endeavor to give an accurate description of the electronic structure and the molecular bonding on a series of neutral and reduced complexes by means of density functional theory (DFT/BP86) calculations (see Computational methods), which is already established to be valuable in determining the electronic structures, the geometrical parameters, bonding analysis and other properties from previous theoretical works of mono-metallic complexes [21-26], and reproducing efficiently the experimental structures.

Experimental

General considerations

All chemicals reagents and solvents were of analytical grade and were used as received. ^1H -NMR and ^{13}C -NMR spectra were recorded on Brüker Avance DPX250 spectrometers. The melting point was determined using an Electrothermal IA9100 digital melting point apparatus. UV spectra were recorded on UV/VIS Spectrophotometer Optizen 1220; IR spectra were recorded on Shimadzu FT/IR-8201 PC spectrophotometer.

Synthesis of ligands

The bis((1*H*-benzo[d]imidazol-2-yl)methyl)sulfane: Ligand (bbms)

The bis((1*H*-benzo[d]imidazol-2-yl)methyl)sulfane (bbms) was prepared according to modified literature methods [27], by using a mixture of 2-mercaptomethylbenzimidazole (164.2 mg, 1 mmol) and 2-chloromethylbenzimidazole (166.6 mg, 1 mmol) in MeOH and in presence of MeONa (81 mg, 1.5 mmol). The cooled precipitates were collected by filtration. Yield 67%; Yellow solid; m.p. 240 °C (m.p. 221 °C [28]); IR spectrum (KBr, $\nu\text{ cm}^{-1}$): 3409, 2781, 2360, 1635, 1535, 1442, 1272, 1157, 1026, 856, 735; ^1H NMR (250.13 MHz, DMSO-*d*6) δ : 12.59 (s_L, 2H), 7.56-7.53 (m, 4H), 7.20-7.16 (m, 4H), 4.08 (s, 4H); ^{13}C NMR (62.9 MHz, DMSO-*d*6) δ : 151.8, 138.8, 121.8, 114.9, 28.8.

The 2-((1*H*-benzo[d]imidazol-2-yl)methylthio)-1*H*-benzo[d]imidazole: Ligand (btmb)

The 2-((1*H*-benzo[d]imidazol-2-yl)methylthio)-1*H*-benzo[d]imidazole (btmb) was prepared according to literature methods [29], by using a mixture of 2-mercaptobenzimidazole (150.2 mg, 1 mmol) and 2-chloromethylbenzimidazole (166.6 mg, 1 mmol) in MeOH and in presence of MeONa (81 mg, 1.5 mmol). A yellow precipitate was formed, filtered and washed with methanol. Yield 77%; Yellow solid; m.p. > 250°C (m.p. 250-257 °C [29]); IR spectrum (KBr, $\nu\text{ cm}^{-1}$): 3429, 2781, 1616, 1500, 1535, 1411, 1357, 1272, 1222, 856, 744; ^1H NMR (250.13 MHz, DMSO-*d*6) δ : 7.55-7.46 (m, 4H), 7.20-7.11 (m, 4H), 4.78 (s, 2H); ^{13}C NMR (62.9 MHz, DMSO-*d*6) δ : 152.9, 149.3, 140.7, 139.5, 125.3, 122.2, 116.5, 114.5, 32.5.

Synthesis of complexes

Synthesis of complex {Co(bbms)Cl₂} (1)

CoCl₂·6H₂O (1 mmol) were added with stirring to a solution of bbms (1 mmol) in 8 mL of MeOH. The mixture was stirred for 18 hours. The blue precipitate **1** that formed was filtered and dried in vacuo. Yield = 84%; m.p.=285-288°C; IR spectrum (KBr, $\nu\text{ cm}^{-1}$): 3444, 2356,

1631, 1527, 1450, 1388, 1272, 1145, 1122, 1037, 744; UV-Vis (chloroform, λ (nm)): 220, 248, 276; Suitable crystals for X-ray diffraction of **1** were obtained from cold dimethylformamide solution.

Synthesis of complex {Zn(bbms)Cl₂} (**2**)

The synthetic procedure of **2** was similar to that for **1**, except that ZnCl₂ (1 mmol) was used instead of cobalt chloride. The yellow solid **2** was obtained in 79% yield. m.p.=285°C; ¹H NMR (250 MHz, DMSO-*d*₆) δ : 13.72 (s_L, 2H), 8.32 (s_L, 2H), 6.9 (s_L, 2H), 7.43-7.40 (m, 4H), 4.07 (s, 4H); ¹³C NMR (62.9 MHz, DMSO-*d*₆) δ : 151.75, 139.1, 132.96, 124.34, 123.39, 118.28, 112.59, 25.13; IR spectrum (KBr, ν cm⁻¹): 3436, 3174, 3136, 2773, 2360, 1608, 1527, 1454, 1415, 1276, 1153, 752; UV-Vis (chloroform, λ (nm)): 224, 246, 276; Suitable crystals for X-ray diffraction of **2** were obtained from cold dimethylformamide solution.

Synthesis of complex {Co(btmb)Cl₂} (**3**)

The synthetic procedure of **3** was similar to that for **1**, except that btmb (1 mmol) was used instead of bbms. The blue solid **3** in 81 % yield was obtained. m.p. > 300°C; IR spectrum (KBr, ν cm⁻¹): 3444, 2985, 2360, 1624, 1415, 1276, 1222, 1149, 1056, 1013, 752. UV-Vis (chloroform, λ (nm)): 226, 250, 286; Suitable crystals for X-ray diffraction of **3** were obtained from cold dimethylformamide solution.

Synthesis of complex {Zn(btmb)Cl₂} (**4**)

The synthetic procedure of **4** was similar to that for **1**, except that btmb (1 mmol) ZnCl₂ (1 mmol) were used instead of bbms and CoCl₂, respectively. The yellow solid **4** in 80 % yield was obtained. m.p > 300 °C; ¹H NMR (250.13 MHz, DMSO-*d*₆) δ : 7.91 (s_L, 4H), 7.39-7.33 (s_L, 4H), 4.88 (s, 2H); IR spectrum (KBr, ν cm⁻¹): 3456, 2333, 1624, 1535, 1419, 1276, 1226, 1153, 1056, 991, 910, 748. UV-Vis (chloroform, λ (nm)): 228, 282; Suitable crystals for X-ray diffraction of **4** were obtained from cold dimethylformamide solution.

X-ray crystallography

The crystal was coated with Paratone oil and mounted on loops for data collection. X-ray data were collected with a Bruker Apex II CCD area detector diffractometer with a graphite-monochromated Mo-K α radiation source (0.71073 Å) at 298 K. The reported structure was solved by direct methods with SIR2002 [30] to locate all the non-H atoms which were refined anisotropically with SHELXL97 [31] using full-matrix least-squares on F² procedure from within the WinGX [32] suite of software used to prepare material for publication.

All absorption corrections were performed with the SADABS program [33]. All the H atoms were placed in the calculated positions and constrained to ride on their parent atoms. The DIAMOND package and ORTEP-3 for Windows programs were used for generating figures of structures [34,35]. Crystal data, structure refinement parameters, some intra and intermolecular interactions hydrogen bonds, C-H... π and π - π stacking for compound **1-4** are listed in Tables 1, 2 and 3.

Corrosion inhibition measurements

Preparation of Solutions

The acid solution of 0.5 M H₂SO₄ was prepared by dilution of analytical grad 97-98% with distilled water. The concentration of the inhibitors employed was 5×10^{-3} M.

Steel Specimen

For galvanostatic and potentiodynamic polarization measurements were performed using a cylindrical working electrode embedded with epoxy steel resin with an exposed surface area of 0.64 cm². The chemical elements content of the working electrode was determined using Philips Analytical MagiX-PRO X-ray Fluorescence Spectrometer (XRF) with the PW2540 vrc sample changer and SuperQ analytical software package. The relative percentage of the elements content is: Al (0.919%), Si (0.351%), P (0.023%), S (0.048%), Mn (0.524%), Cu (0.938), Fe (97.197%). Before measurement, the working electrode was abraded with different emery paper, from a coarse grade 400 and proceeding in steps to fine grade 2000, degreased with ethanol, rinsed several times with distilled water, then dried.

The electrochemical measurements were carried out in a conventional cylindrical glass cell equipped with a three-electrode system that consisted of a working electrode, a platine counter electrode and a saturated calomel electrode (SCE) as the reference electrode.

Polarization and impedance measurements were performed using a potentiostat/galvanostat/ZRA «GAMRY-Reference 3000». The electrochemical cell was kept for 30 minutes to stabilize the steady-state potential before the EIS and potentiodynamic polarization measurements were started. The polarization measurements were performed using a scan rate of 1 mV s⁻¹ in the potential range of -800 to -200 mV. Electrochemical impedance spectroscopy (EIS) were performed at open circuit potential (E_{corr}) over a frequency range of 10 kHz to 10 mHz with AC signals of 10 mV peak-to-peak amplitude at the open circuit potential. Various corrosion parameters and inhibition efficiency (IE %) are listed in Tables 5 and 6.

Antimicrobial activity

The antimicrobial activity the prepared complexes **1-4** were evaluated *in vitro* for their antimicrobial activity against *Staphylococcus aureus* : Sa (ATCC-25923), *Klebsiella pneumonia* Kp (ATCC-700603), *Pseudomonas Syringae* Ps (Kc 311253) and *Pichia caribbica* Pc (Kc 977491) as yeast. The two ligands bbms and bmtb were used for comparison. Solid tablet of the tested compounds were used in this study and are prepared as follow: The tested compound (1 mg) is added to 100 mg of peptone as adsorbing agent, and then finely ground and mixed in a smooth agate mortar. This mixture is placed in special 6 mm evacuable pellet die, and then compacted under pressure of 1.5 Tons. Solid tablet of 6 mm diameter and a thickness of about 0.5 mm are obtained and are used within 60 minutes. Microbial cells were swabbed on to nutrient medium (Mueller–Hinton Broth for bacteria and YPG Medium for yeast) in petri plates and the solid tablet containing different compounds were placed onto the agar using sterile forceps. The inoculated petri plates were incubated at 37 °C and 30 °C for 24 h for bacterial and yeast strains, respectively. Finally, the diameters of the inhibition zone around each pellet were measured in millimeter. For comparison of benzylpenicilline sodique (1 mg), adsorbed on 100 mg of peptone, was used as standard drug. The results of the antimicrobial screening of the prepared compounds are listed in Table 7.

Computational methods

Density functional theory (DFT) calculations were carried out on the studied compounds using the Amsterdam Density Functional (ADF) program [36], developed by Baerends and co-workers [37-41]. Electron correlation was treated within the local density approximation (LDA) in the Vosko–Wilk–Nusair parametrization [42]. The non-local corrections of Becke and Perdew (BP86) were added to the exchange and correlation energies, respectively [43-46]. The numerical integration procedure applied for the calculations was developed by te Velde et al.⁴¹ The atom electronic configurations were described by a triple- ζ Slater-type orbital (STO) basis set for H 1s, C 2s and 2p, N 2s and 2p augmented with a 3d single- ζ polarization for C and N atoms and with a 2p single- ζ polarization for H atoms. A triple- ζ STO basis set was used for the Co and Zn transition metals 3d and 4s, augmented with a single- ζ 4p polarization function for Co and Zn. A frozen-core approximation was used to treat the core shells up to 1s for C, N, 3p for Co and Zn transition metals.³⁷⁻⁴¹ Full geometry optimizations were carried out using the analytical gradient method implemented by Versluis and Ziegler [47]. Spin-unrestricted calculations were performed for all the open-shell systems. Frequencies calculations [48,49] were performed on all the studied compounds to check that

the optimized structures are at local minima. Representation of the molecular structures and molecular orbitals were done using ADF-GUI [36].

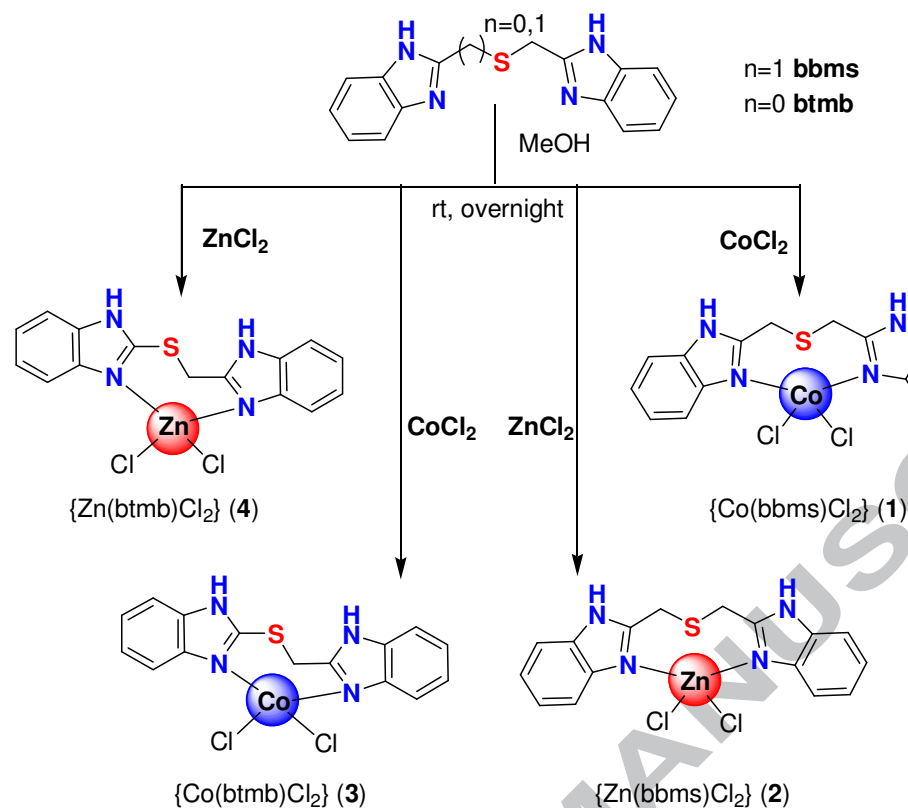
Results and discussion

Synthesis

The bis((1*H*-benzo[d]imidazol-2-yl)methyl)sulfane (bbms) was synthesized following a modified literature procedure starting from 2-chloromethylbenzimidazole and 2-mercaptomethylbenzimidazole [27]. The 2-((1*H*-benzo[d]imidazol-2-yl)methylthio)-1*H*-benzo[d]imidazole (btmb) was prepared according to literature procedure starting from 2-mercaptobenzimidazole and 2-chloromethylbenzimidazole and its structure has been confirmed by spectroscopic methods [29].

The complexes **1-4** have been reported previously in a few papers and their structures were proposed spectroscopically or theoretically in other some cases [50-54]. However, no structural confirmation using crystallographic study had been reported. Thus it was considered of interest, in order to confirm and understand the three dimensional structures of these complexes, to carry out an X-ray diffraction analysis. In this context, we have adopted the following procedure for their preparation:

The ligands bbms and btmb were stirred in MeOH with MCl_2 (1 equivalent of $M=Co, Zn$) overnight at room temperature (Scheme 1). The solids metal (II) complexes were filtered off and dried. All complexes are stable in the air, soluble in DMF and DMSO but insoluble in water and other organic solvents. The organic part of complexes **2** and **4** were also confirmed by 1H and ^{13}C NMR. Crystals of complexes **1, 2, 3** and **4** were obtained by recrystallization in DMF and the complexes structures are shown in Scheme 1 and Figure 1a-d.



Scheme 1. Synthesis of complexes **1**, **2**, **3**, and **4**

Crystal structures

All complexes were recrystallized and suitable crystals of **1**, **2**, **3** and **4** were grown in DMF solution of the corresponding complexes. The X-ray crystallographic analysis confirmed their respective structures and the refined X-ray crystal structures are shown in Figures 1a-d.

Crystal data and structural details of the prepared complexes are presented in Table 1.

Table 1

Crystallographic data and refinement parameters for **1-4**.

	{Co(bbms)Cl ₂ } (1)	{Zn(bbms)Cl ₂ } (2)	{Co(btmb)Cl ₂ } (3)	{Zn(btmb)Cl ₂ } (4)
Formula	C ₁₆ H ₁₄ N ₄ SCl ₂ Co	C ₁₆ H ₁₄ N ₄ SCl ₂ Zn	C ₁₅ H ₁₂ N ₄ SCl ₂ Co	C ₁₅ H ₁₂ N ₄ SCl ₂ Zn
Formula weight	424.2	430.64	410.18	416.64
Crystal habit, color	Prism, Blue	Needle, Colorless	Prism, Blue	Block, Colorless
Crystal system	Orthorhombic	Orthorhombic	Monoclinic	Monoclinic
Space group	P bca	P bca	P 2 ₁	P 2 ₁
a (Å)	14.0899(7)	14.1241(3)	8.1661(16)	8.2890(5)
b (Å)	15.1625(6)	15.1797(3)	13.762(3)	13.8148(8)
c (Å)	15.8182(7)	15.8011(3)	14.614(3)	14.6318(9)
α (°)	90	90	90	90
β (°)	90	90	92.468(12)	92.058(4)

γ (°)	90	90	90	90
Volume (Å ³)	3379.4(3)	3387.75(12)	1640.9(6)	1674.42(17)
Z, Z'	8, 8	8, 8	2, 4	2, 4
Density (calculated, g cm ⁻³)	1.668	1.689	1.661	1.653
Absorption coefficient (mm ⁻¹)	1.46	1.894	1.501	1.913
F(000)	1720	1744	828	840
Crystal size (mm)	0.09×0.14×0.15	0.03×0.04×0.13	0.11×0.15×0.19	0.09×0.11×0.14
θ range for data collection (°)	2.36 - 25.04	2.58-27.71	2.79 - 31.06	2.46- 26.37
Reflections collected	20250	16920	17080	13897
Independent reflections	4031	3956	8836	6479
R _{int}	0.0512	0.0302	0.0428	0.0403
Reflections with $I \geq 2\sigma(I)$	2873	3060	7210	5128
Number of parameters	217	217	423	409
Goodness-of-fit on F^2	1.141	1.041	0.981	1.077
Final R indices [$I \geq 2\sigma(I)$]	0.0514	0.0318	0.0382	0.0722
R indices [all data]	$R_1=0.0907$,	$R_1=0.0471$,	$R_1=0.0539$,	$R_1=0.0911$,
Largest difference peak and hole (Å ⁻³)	$wR_2=0.1027$	$wR_2=0.0777$	$wR_2=0.0835$	$wR_2=0.1913$
Flack's Parameter	--	--	0.017(11)	0.12(2)
CCDC deposition no.	CCDC 1432478	CCDC 1432480	CCDC 1432479	CCDC 1432481

Crystal structure of {Co(bbms)Cl₂} (1) and {Zn(bbms)Cl₂} (2)

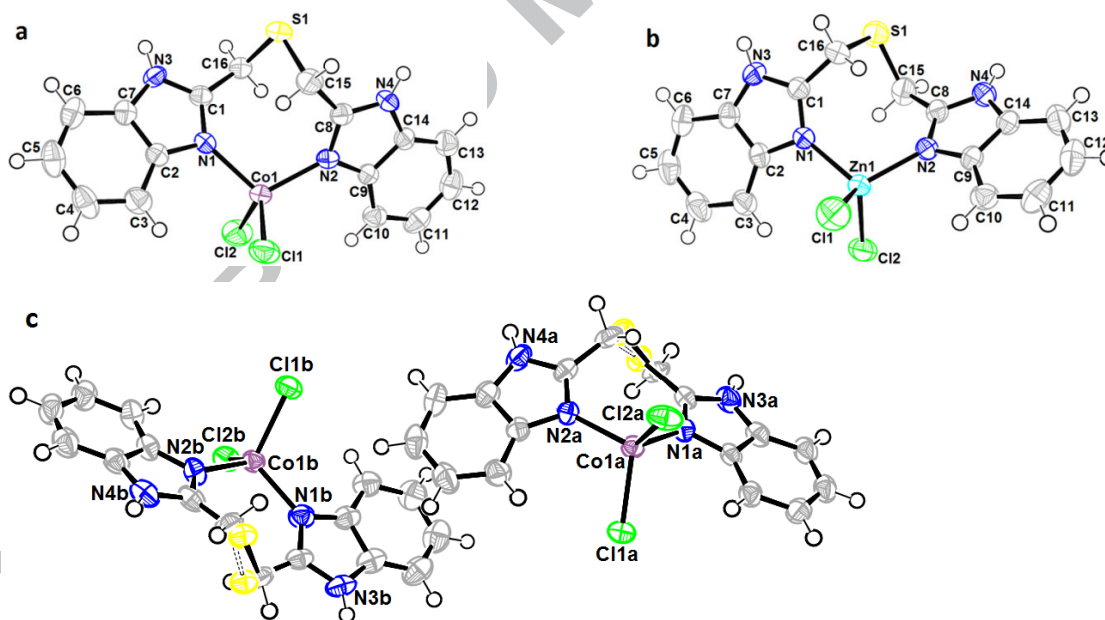
The complex **1** crystallizes in the orthorhombic crystal system (space group Pbc_a). The compound {Co(bbms)Cl₂} (1) (Figure 1a) is a tetra-coordinate metal complex. The complex contains one organic ligand of bis((1*H*-benzo[d]imidazol-2-yl)methyl)sulfane and the cobalt (II) is surrounded by two N-donor atoms and two chloride ligand. The cobalt(II) environment exhibits a quasi-regular tetragonal coordination. The bond distances Co(1)–N(1) and Co(1)–N(2) are 2.046 (4) Å and 2.036 (4) Å, respectively, while the distance Co(1)–Cl(1) is 2.2525 (16) Å and the distance Co(1)–Cl(2) is 2.2507 (15) Å. Bond angles for N(1)–Co(1)–Cl(1) and for Cl(1)–Co(1)–Cl(2) are 115.66 (12)° and 109.65 (6)°, respectively and the bond angle N(1)–Co(1)–N(2) is 109.46 (16)° (Table 1). The deviation of these values from the ideal 109° corresponding to a perfect tetragonal geometry indicates a distorted tetragonal geometry. Bond lengths and angles are in the expected range [55-57].

In bis((1*H*-benzo[d]imidazol-2-yl)methyl)sulfane ligand, both benzimidazole rings, linked by thiomethyl group, are quasiplanar and form between each other a dihedral angle of 44.74 (11)°. The crystal packing can be described as alternating double layers along the b axis (at $b=1/4$ and $b=3/4$) parallel to (010) plane (Figure 2). These layers are connected with N-H...Cl and C-H...S interactions resulting in the formation of two dimensional networks. Hydrogen bond

between amine moieties and chlorine atom form a chain with $C_1^1(6)$ graph set motif [58,59]. Additional hydrogen-bonding parameters are listed in Table 2.

The packing is consolidated by slippest π - π stacking with centroid to centroid distance of 3.601 (3) Å to 3.753 (3) Å and a weak intermolecular interaction C(12)-H(12)...Cg (N(1)-C(1)-N(3)-C(7)-C(2)) with a distance of C...Cg is 3.660 (6) Å and the C-H...Cg angle of 133° (Table 3). These interactions link the molecule within the layers and also link layers together and reinforcing the cohesion of the complex structure.

Compounds **1** and **2** are isostructure (Table 1). The asymmetric unit of **2** consists of bbms ligand binds to one zinc(II) through the two amine nitrogen atoms (Figure 1b). The zinc atom is tetrahedrally surrounded also by two chlorine atoms. The two chlorine atoms are said to be joined by a covalent bond. The molecular structure is running in zigzag chain along the a axis. The network is stabilized by two intermolecular interactions N-H...Cl between Cl atoms and H atoms of N atoms of the nearest benzimidazole ring. Similarly, in this compound, a weak C-H...Cl intramolecular interactions hydrogen bonds (Figure 3), C-H... π intermolecular interactions and π - π stacking are observed (Table 2 and 3).



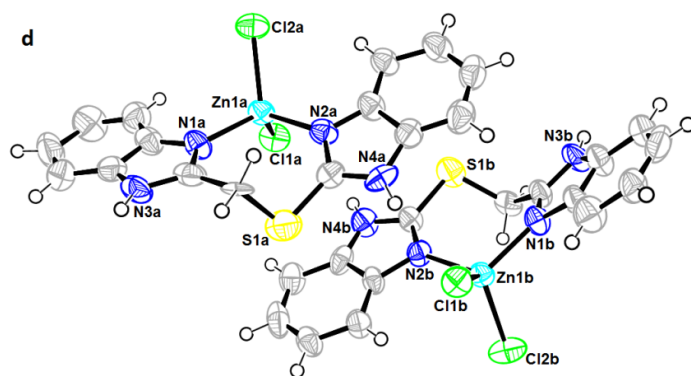


Fig. 1. Oak ridge thermal ellipsoid plots (ORTEP) of the molecular structures of **1**, **2**, **3** and **4** in the crystal and atom numbering scheme adopted (displacement ellipsoids at the 50 % probability level; H atoms with arbitrary radii; blue: nitrogen, yellow: sulfur, green: chlorine).

Crystal structure of $\{\text{Co}(\text{btmb})\text{Cl}_2\}$ (**3**) and $\{\text{Zn}(\text{btmb})\text{Cl}_2\}$ (**4**)

In **3**, the compound crystallizes in the monoclinic crystal system (space group $P2_1$) (Table 1, Figure 1c). There are two crystallographic independent but similar molecules in the asymmetric unit that we have labeled as molecule a and b (Figure 1c and Figure 4). The btmb ligand who act as bidentate chelating ligand, consists of two benzimidazole unit attached together with thiomethyl linker. Both molecules of $\text{Co}(\text{btmb})\text{Cl}_2$ (**3**) are refined with disordered atoms of sulfur and carbon neighbors in the chain. Changes in a linker moiety, such as methylthiomethyl vs thiomethyl, had a significant effect on the dihedral angles values between the two benzimidazole entities (for compound **1**: $44.74(11)^\circ$; for compound **3**: $29.62(5)^\circ$ in molecule a and $22.29(6)^\circ$ in molecule b).

In the asymmetric unit of **3**, the Co(II) is in slightly distorted tetrahedral environment. It is surrounded by two N atoms from benzimidazole ring of organic ligand (Co(1a)-N(1a) = $2.019(2)$ Å; Co(1a)-N(2a) = $1.998(3)$ Å; Co(1b)-N(1b) = $2.000(3)$ Å; Co(1b)-N(2b) = $1.999(3)$ Å) and two chlorine atoms [Co(1a)-Cl(1a) = $2.2622(9)$ Å; Co(1a)-Cl(2a) = $2.2430(9)$ Å; Co(1b)-Cl(1b) = 2.2607 Å; Co(1b)-Cl(2b) = $2.2501(9)$ Å].

The structure of **3** is refined with disorder between S and C atoms with 0.37/0.63 ratio, using part instruction of Shelx program [31]. The site occupancies of the major and minor components of the disordered carbon and sulfur atoms are 0.37 and 0.63, respectively.

Compounds **3** and **4** are isostructure (Figure 1d). There are two crystallographic independent molecules (Figure 1d). Complex **4**, with a bidentate N donors ligand and two bounds chlorines, possess a quasi-regular tetrahedral geometry about the Zn(II) centre with [Cl(1a)–

Zn(1a)–Cl(2a): 107.52(9)°; N(1a)–Zn(1a)–N(2a): 110.5(3)°; N(1a)–Zn(1a)–Cl(1a): 110.7(2); Cl(1b)–Zn(1b)–Cl(2b): 112.39(9); N(1b)–Zn(1b)–N(2b): 108.8(3)°; N(1b)–Zn(1b)–Cl(1b): 110.43(19)°]. The ligand coordinates with the metal centre in its neutral form. Bond lengths and angles are in the expected range [55-57]. Various intermolecular interactions such as N–H...Cl, C–H... π and π - π contribute in the stability of the crystal packing (Figure 5, Tables 2 and 3).

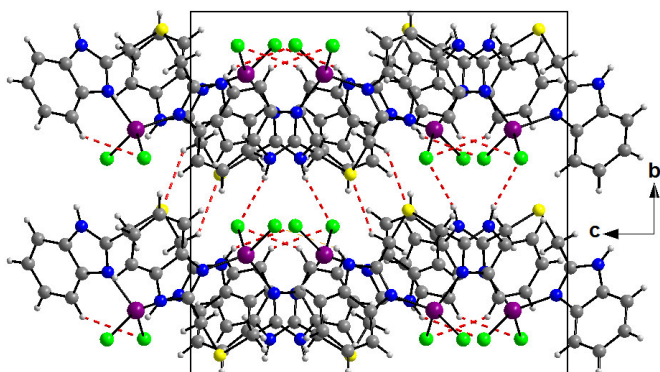


Fig. 2. Alternating layers parallel to (010) plane of **1** at $b=1/4$ and $b=3/4$, viewed via a axis. Hydrogen bonds are shown as red dashed lines (N–H...Cl and C–H...S) connecting these layers.

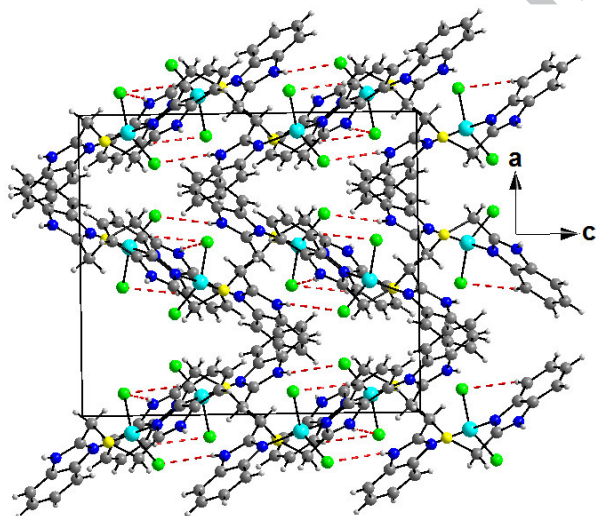


Fig. 3. View of the crystal structure of **2** showing layers in zigzag along the a axis. Hydrogen bonds are shown as red dashed lines (N–H...Cl) connecting these layers.

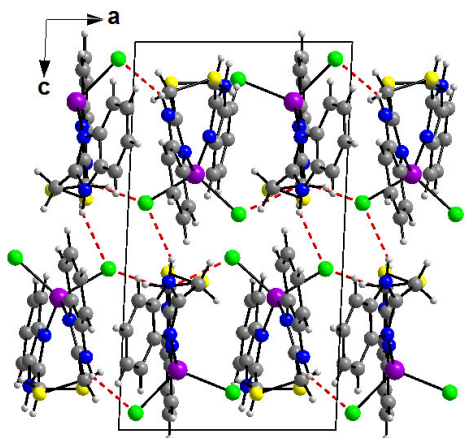


Fig. 4. View of the crystal structure of **3** showing double layers along the *c* axis connecting via hydrogen bonds interactions shown as red dashed lines.

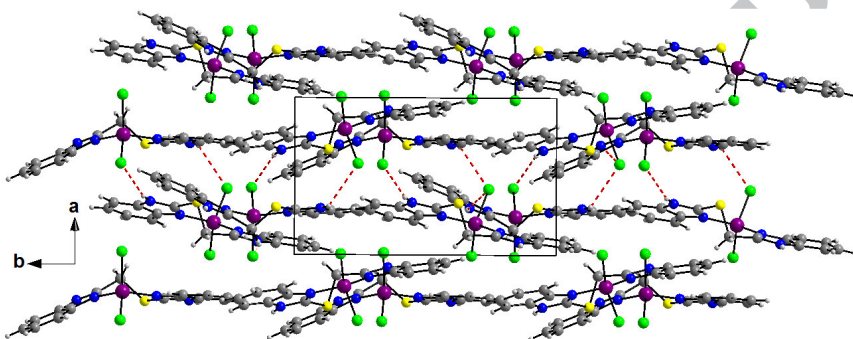


Fig. 5. Crystal packing of **4** viewed via *c* axis showing hydrogen bond, between layers, as dashed lines.

Table 2

Distances (Å) and angles (°) of hydrogen bond for **1**, **2**, **3** and **4**.

D–H...A	<i>d</i> (D–H)	<i>d</i> (H...A)	<i>d</i> (D–A)	D–H–A	Symmetry
Compound 1					
N(3)–H(3N)...Cl(1)	0.86	2.78	3.527(5)	146	$x, 1/2-y, -1/2+z$
N(4)–H(4N)... Cl(2)	0.86	2.37	3.204(5)	163	$1-x, -1/2+y, 3/2-z$
C(10)–H(10)... Cl(2)	0.93	2.76	3.506(5)	138	x, y, z
C(16)–H(11a)...S(1)	0.97	2.86	3.654(5)	139	$-1+x, y, z$
Compound 2					
N(3)–H(3N)...Cl(2)	0.86	2.37	3.204(2)	163	$2-x, -1/2+y, 3/2-z$
N(4)–H(4N)... Cl(1)	0.86	2.77	3.523(1)	147	$x, 1/2-y, -1/2+z$
C(3)–H(3)... Cl(2)	0.93	2.74	3.492(3)	138	x, y, z
Compound 3					
N(4a)–H(4aN)...Cl(1b)	0.86	2.63	3.280(3)	133	$-x, -1/2+y, 1-z$
N(3b)–H(3bN)...Cl(2a)	0.86	2.37	3.211(3)	164	$-x, 1/2+y, 2-z$
N(3a)–H(3aN)...Cl(1b)	0.86	2.81	3.372(3)	125	$x, -1+y, z$
N(4a)–H(4aN)...Cl(2b)	0.86	2.82	3.281(3)	115	$1+x, -1+y, z$

N(4b)–H(4bN)...Cl(1a)	0.86	2.45	3.238(3)	152	-x,-1/2+y,1-z
Compound 4					
N(4a)–H(4aN)...Cl(1b)	0.86	2.48	3.266(8)	152	x, y, z
N(4b)–H(4bN)...Cl(1a)	0.86	2.81	3.388(9)	126	x, y, z
N(3b)–H(3bN)...Cl(1a)	0.86	2.62	3.283(8)	135	1-x,1/2+y,2-z
N(3a)–H(3aN)...Cl(2b)	0.86	2.39	3.220(8)	163	1-x,-1/2+y,1-z

Table 3

Intermolecular and intramolecular interactions C–H...Cg (C–H... π ; Å, °) operating in the crystal structure of **1**, **2**, **3** and **4** (Å, °).

C–H...Cg	<i>d</i> (C–H)	<i>d</i> (H...Cg)	<i>d</i> (C–Cg)	C–H...Cg	Symmetry
Compound 1					
C(12)–H(12)...Cg1 (N(1)/C(1)/N(3)/C(7)/C(2))	0.93	2.96	3.660(6)	133	-1/2+x,y,3/2-z
Compound 2					
C(5)–H(5)...Cg2 (N(2)/C(8)/ N(4)/C(14)/ C(9))	0.93	2.97	3.671(3)	133	1/2+x,y,3/2-z
Compound 3					
- C(5b)–H(52)...Cg3 (N(2a)/C(8a)/N(4a)/C(14a)/C(9a))	0.93	2.97	3.332(4)	105	-1+x,y,z
- C(151)–H(91b)...Cg4 (C(2a)/C(3a)/C(4a)/C(5a)/C(6a)/C(7a))	0.97	2.62	3.346(7)	132	-1+x,1+y,z
- C(171)–H(92a)...Cg5 (C(9b)/C(10b)/C(11b)/C(12b)/C(13b)/C(14b))	0.97	2.94	3.644(7)	130	1+x,-1+y,z
- C(152)–H(91d)...Cg4 (C(2a)/C(3a)/C(4a)/C(5a)/C(6a)/C(7a))	0.97	2.60	3.253(13)	125	x,1+y,z
- C(172)–H(92b)...Cg5 (C(9b)/C(10b)/C(11b)/C(12b)/C(13b)/C(14b))	0.97	2.69	3.640(7)	168	x,-1+y,z
Compound 4					
- C(5a)–H(5a)...Cg6 (N(1b)/C(1b)/ N(3b)/C(7b)/ C(2b))	0.93	2.90	3.376(15)	113	1+x,-1+y,z
- C(15a)–H(15b)...Cg7 (C(9b)/C(10b)/ C(11b)/C(12b)/ C(13b)/ C(14b))	0.97	2.80	3.388(8)	120	1+x,y,z
- C(15b)–H(15c)...Cg8 (C(9a)/C(10a)/ C(11a)/C(12a)/ C(13a)/ C(14b))	0.97	2.97	3.664(9)	128	-1+x,y,z

Computational investigation

In order to provide a better understanding of the bonding and the electronic structure of the {Co(bbms)Cl₂} (**1**), {Zn(bbms)Cl₂} (**2**), {Co(btmb)Cl₂} (**3**) and {Zn(btmb)Cl₂} (**4**) complexes, we have carried out DFT calculations. Calculations have been performed without any symmetry constraints on the neutral and on the mono-reduced forms of **1** and **3** species (Figures 6 and 7), but only on the neutral of **2** and **4** ones. Selected computed data for the obtained structures are given in Tables 4. Full geometry optimizations of **1** and **3** show that the Co(II) metal cation is in a tetrahedral environment as an ML₄ complexes having a 15-MVE (metal valence electrons) configuration. Indeed, the average Co–N bond distances of

2.042 and 2.028 Å and the average Co-Cl bond distances of 2.242 and 2.250 Å, obtained for **1** and **3**, respectively, are comparable to those obtained experimentally (Table 4). The N-Co-N bond angles of 110 and 112° computed for **1** and **3** complexes, respectively, are close to the experimental ones of 109°, while the calculated Cl-Co-Cl of 132 and 128° are larger than the experimental ones. The spin density values of 0.95 and 0.95 obtained for **1** and **3** show the localisation of the unpaired electron on the Co(II) center as d^7 metal in both cases. The singly occupied molecular orbital 68a (SOMO) is mainly metallic of (75% composed of d_{xy} and d_{yz}) and 65a (57% composed of $d_{x^2-y^2}$) for **1** and **3**, respectively, as displayed in Figure 7 showing that the reduction will occur on the metal and will affect its oxidation state. We have optimized the geometries of the **1**[•] and **3**[•] models in their singlet (**1**[•](S) and **3**[•](S)) and triplet (**1**[•](T) and **3**[•](T)) states corresponding to Co(I) center. Indeed, the reduced **1**[•] and **3**[•] species in their triplet state are more stable than the single ones by 22.4 and 9.4 kcal mol⁻¹, respectively. Indeed, the one electron reduction decreases the oxidation state and the cobalt center becomes Co(I) d^8 center instead of Co(II) d^7 one. The structures of the reduced **1**[•](S) and **3**[•](S) forms (Figure 7) exhibit moderate but significant HOMO-LUMO gaps of 0.61 and 1.06 eV (Figure 8), respectively. Surprisingly, **1**[•](S) complex adopts different structure than the neutral one, wherein the metal environment undergoes remarkable structural modification associated with Cl-Co-Cl and N-Co-N bond angles opening of 163 and 148°, respectively, tending towards the linearity, and thus giving rise to a quasi-square planar ML₄ geometry with a 16-MVE configuration. Moreover, the NCINCl dihedral angle of 19° deviates slightly from the planarity. Whereas for the **3**[•](S) and **3**[•](T) structures, one can observe a remarkably structural modification corresponding to a C-S bond rupture of the (CH)₂-S bridge leading to positive interactions between cobalt and sulphur atoms highlighted by a short Co-S distance of 2.556 Å for **3**[•](S) species.

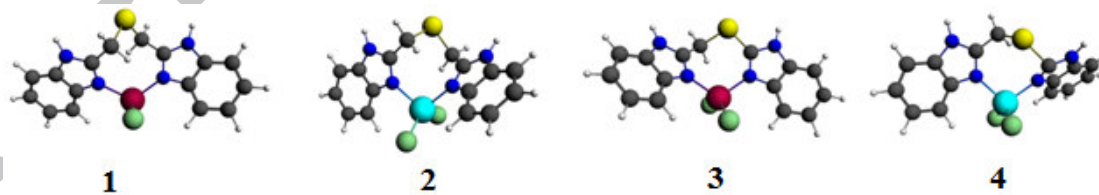


Fig. 6. Optimized structures of complexes **1**, **2**, **3** and **4**.

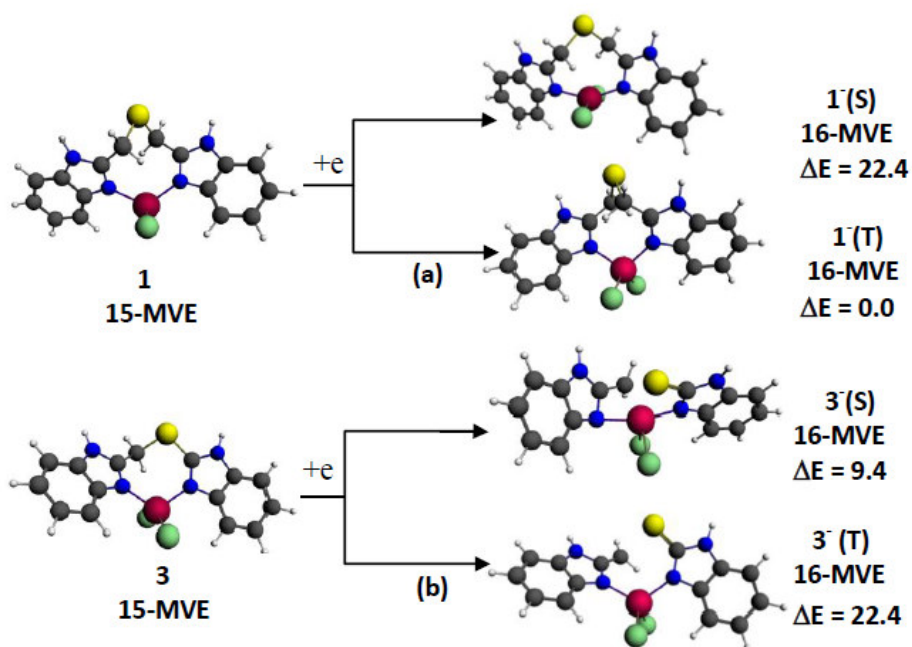


Fig. 7. Reduction mechanisms for neutral **1** (a) and **3** (b) complexes of 15-MVE giving rise to singlet and triplet species of 16-MVE.

Table 4

Selected parameters obtained for neutral and reduced complexes. Experimental bond distances are given in parentheses.

	{Co(bbms)Cl ₂ }	{Co(bbms)Cl ₂ } ⁻		{Co(btmb)Cl ₂ }	{Co(btmb)Cl ₂ } ⁻		{Zn(bbms)Cl ₂ }	{Zn(btmb)Cl ₂ }
	S = 1/2	S = 0	S = 1	S = 1/2	S = 0	S = 1	S = 0	S = 0
	1	1⁻(S)	1⁻(T)	3	3⁻(S)	3⁻(T)	2	4
MVE	15	16	16	15	16	16	18	18
ΔE (kcal mol ⁻¹)	-	22.4	0.0	-	9.4	0.0	-	-
HOMO-LUMO gap (eV)	-	0.61	-	-	1.06	-	3.18	3.13
Average M-N (Å)	2.042 (2.041)	1.907	2.025	2.028 (2.009)	1.972	2.038	2.146	2.143
Average M-Cl (Å)	2.242 (2.253)	2.273	2.303	2.250 (2.251)	2.294	2.263	2.241	2.171
N-M-N (°)	110 (112)	148	106	112 (112)	164	115	104 (109)	97 (109)
Cl-M-Cl (°)	132 (109)	163	126	128 (109)	94	114	127 (110)	125 (113)
Spin density	0.95	-	2.19	0.95	-	2.08	-	-

Both {Zn(bbms)Cl₂} (**2**) and {Zn(btmb)Cl₂} (**4**) structures exhibit large HOMO-LUMO gaps of 3.18 and 3.13 eV, respectively, satisfying the 18-electron configuration and synonymous of good kinetic and thermodynamic stabilities. The optimized average Zn-Cl and Zn-N bond

distances of 2.241 and 2.146 Å, respectively, obtained for **2** are comparable to those obtained for **4** of 2.171 and 2.143 Å, respectively, and comparable to the experimental values (Table 4), while the Cl-Zn-Cl and N-Zn-N bond angles of 127 and 104° obtained for **2** are slightly less open than those obtained for **4** of 125 and 97°, respectively, in accordance with the long and short (CH₂)₂S and (CH₂)S bridge in **2** and **4** complexes, respectively. However, **2** and **4** are considered as tetrahedral ML₄ complexes in consideration of bond angles comparable to those obtained experimentally corresponding to Zn(II) as d¹⁰ metal. For both **2** and **4** complexes, it is worth noting that the three highest occupied MOs are purely chlorine exhibiting neglected metal contributions do not exceed 2%, thus, oxidations and reductions of **2** and **4** will not affect Zn metal and its environment. Noticing that the purely metallic MOs are situated at low energies ranging from -10.86 to -10.52 eV, while the HOMO, HOMO-1 and HOMO-2 which are chlorine orbitals ranging from -5.73 to -5.62 eV.

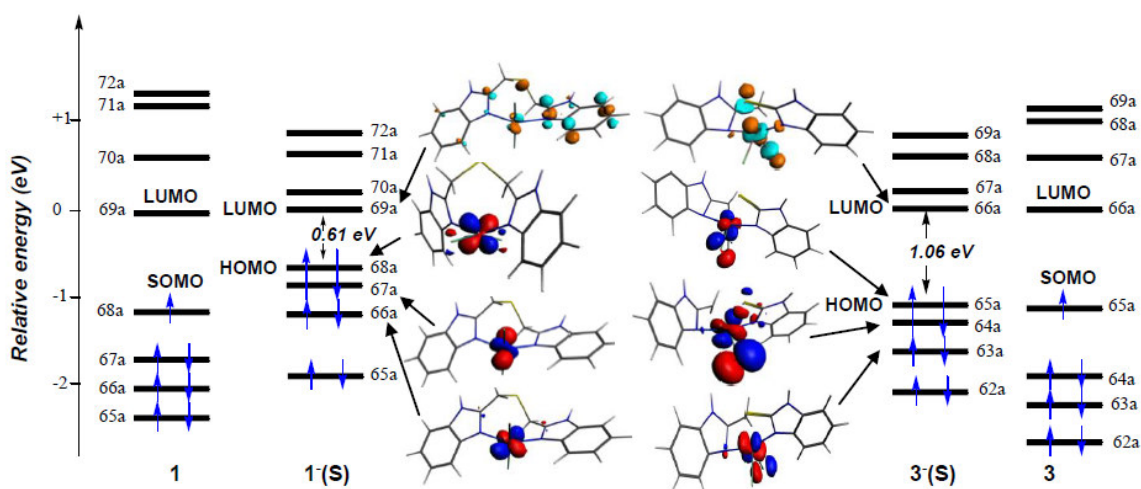


Fig. 8. MO diagrams for neutral **1** and **3** and anionic **3** and **3(S)** species. LUMO energies are set arbitrary to zero for comparison facilities.

Corrosion test

The prepared complexes were subjected to two types of electrochemical measurements in order to evaluate and confirm their abilities to inhibit the corrosion of steel in aqueous acid solutions.

Polarization Measurements

The potentiodynamic polarization curves (Tafel curves) for steel in 0.5 M H₂SO₄ in absence and presence of 5×10⁻³ M of compounds **1**, **2**, **3** and **4** are shown in Figure 9.

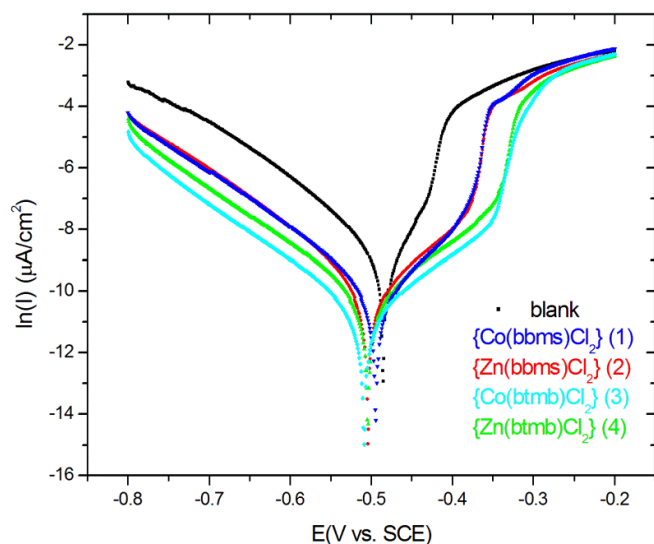


Fig. 9. Polarization curves of steel in 0.5 M H₂SO₄ without and with 5×10^{-3} M of compounds **1-4** at 298 K.

It is clear from Figure 9 that the presence of all inhibitors causes a decrease in the corrosion rate i.e., shifts both anodic and cathodic curves to lower current densities. At the same time, this change is associated with a negative shift in E_{corr} compared with that of the blank solution (not more than 45 mV versus SCE). The results suggest that all compounds act as mixed-type inhibitors for steel in 0.5 M H₂SO₄ solution [60,61].

It should be noted that the cathodic current–potential curves give rise to parallel Tafel lines in the presence and in the absence of the tested compounds. This indicates that the adsorbed inhibitors do not affect the mechanism of hydrogen evolution.⁶² Furthermore, It should be noted that no change in the anodic Tafel slopes are observed in presence of compounds **2** and **4**. However, a slight changes were observed in the case of **1** and **3**, suggests that all compounds doesn't affect considerably the dissolution mechanism of steel.

The corrosion parameters such as corrosion current density (I_{corr}), corrosion potential (E_{corr}), Tafel slopes (ba and bc), surface coverage θ and inhibition efficiency ($IE\%$) are given in Table 5. The surface coverage θ values and the inhibition efficiency were determined from the equation 1 and 2 respectively [60]:

$$IE(\%) = \frac{I_{\text{corr}(0)} - I_{\text{corr}}}{I_{\text{corr}(0)}} \times 100 \quad (1)$$

$$\theta = 1 - \frac{I_{\text{corr}}}{I_{\text{corr}(0)}} \quad (2)$$

The values of the corrosion current density (I_{corr}) and the corrosion potential (E_{corr}) were obtained from the intersection of the anodic and cathodic curves through extrapolation of the Tafel line, where I_{corr} and $I_{corr(0)}$ are the corrosion current density with and without inhibitor in the 0.5 M H_2SO_4 solutions, respectively.

As shown in Table 5, the result shows that all compounds inhibit the corrosion of steel in 0.5 M H_2SO_4 solution and the inhibitive ability increase when btmb was used instead of bsbm. In addition, the nature of metal doesn't have a significant effect in inhibition efficiency. The inhibition efficiency for **3** and **4** were 91.3% and 88.6%, respectively, which is higher than that obtained for **1** (86.5%) and **2** (86.7%) at the same concentration (5×10^{-3} M).

Table 5

Polarization parameters and IE% for steel corrosion in 0.5 M H_2SO_4 without and with 5×10^{-3} M of inhibitors **1-4** at 298 K.

	E_{corr} (mV)	I_{corr} ($\mu A \cdot cm^{-2}$)	ba (mV. dec ⁻¹)	bc (mV. dec ⁻¹)	IE %
Blank	-485	235.1	97.4	135	-
{Co(bbms)Cl ₂ } (1)	-494	31.9	77.9	113.2	86.5
{Zn(bbms)Cl ₂ } (2)	-504	31.0	83.6	107.1	86.7
{Co(btmb)Cl ₂ } (3)	-509	20.1	113.7	119.2	91.3
{Zn(btmb)Cl ₂ } (4)	-504	26.6	98.2	115.8	88.6

Electrochemical impedance spectroscopy measurements

EIS was also used to investigate the adsorption process by calculating the double layer capacitance (C_{dl}) and the charge transfer resistances (R_{ct}) under different conditions [63-65]. Figure 10 shows the Nyquist diagrams for steel in 0.5 M H_2SO_4 in the presence and absence of compounds **1-4**.

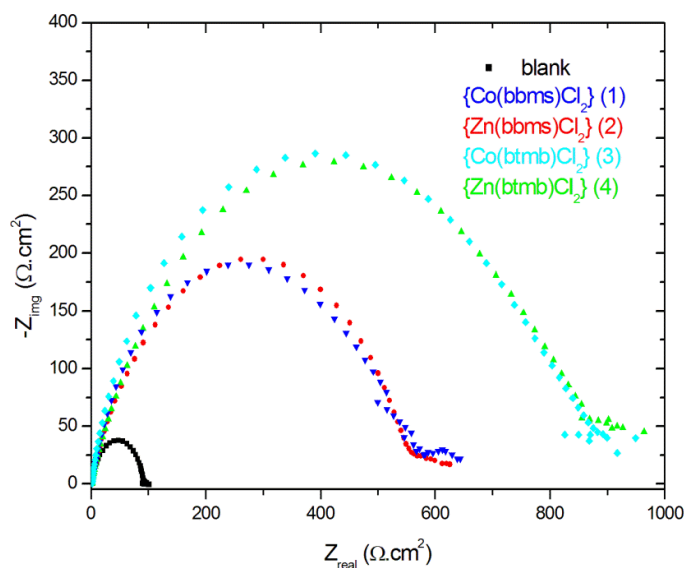


Fig. 10. Nyquist plots for steel in 0.5 M H₂SO₄ solutions without and with 5×10⁻³ M of compounds **1-4** at 298 K.

The impedance spectra in absence and presence of all compounds exhibit a single depressed capacitive loop. Clearly, the capacitive loops in the presence of all compounds are larger than that in the absence of inhibitors (blank solution), which proves that corrosion resistance of steel occurs in presence of these compounds. Furthermore, the diameters of the capacitive loops in the presence of inhibitor **3** and **4** are larger to those obtained in the presence of inhibitor **1** and **2** (Figure 10).

The electrochemical parameters derived from the Nyquist diagram are given in Table 6. The R_s represent the resistance of solution. Double-layer capacitance (C_{dl}) values were calculated using the following equation (3) [66-68].

$$C_{dl} = (Y_0 \times R_{ct}^{(1-n)})^{1/n} \quad (3)$$

Y_0 and n are the magnitude of admittance of the constant phase element (CPE) and the electrode surface roughness/heterogeneity factor, respectively.

Analyze of the impedance results in Table 6 shows that the values of C_{dl} and Y_0 are smaller in the presence of all compounds than in their absence. Complementarily, the values of R_{ct} increase in presence of all compounds. These results suggest that all compounds formed a protective layer on the electrode surface and act as a barrier for charge transfer [69,70].

In other hand, the values of the phase shift n decrease in presence of all compounds, when compared to that obtained in 0.5M H₂SO₄ (0.8898). This shows an increase of the surface inhomogeneity as a result of the inhibitor's adsorption [71].

The inhibition efficiencies for all compounds were calculated using the following equation (4):

$$IE(\%) = \frac{R_{ct} - R_{ct(0)}}{R_{ct}} \times 100 \quad (4)$$

where $R_{ct(0)}$ and R_{ct} are charge transfer resistance in the absence and presence of inhibitor respectively.

From Table 6, the EIS measurements also shows that the all compounds can clearly inhibit the corrosion of steel in 0.5 M H_2SO_4 solution and the inhibition efficiency of the investigated inhibitors increases in the following order: 3 and 4 > 1 and 2. This result is in a good agreement with this obtained from potentiodynamic polarization measurements (Table 5).

Table 6

Impedance parameters and inhibition efficiency for steel in 0.5 M H_2SO_4 without and with 5×10^{-3} M of inhibitors **1-4** at 298 K.

	R_s ($\Omega.cm^2$)	R_{ct} ($\Omega.cm^2$)	n	Y_0 ($S^n.cm^{-2}.\Omega$)	C_{dl} ($\mu F.cm^{-2}$)	IE %
Blank	2.606	89.55	0.8898	152.2	89.4	-
{Co(bbms)Cl ₂ } (1)	1.430	543.7	0.8038	55.9	23.8	83.5
{Zn(bbms)Cl ₂ } (2)	2.139	554.1	0.7803	130.2	62.1	83.8
{Co(btmb)Cl ₂ } (3)	1.562	798.1	0.8387	46.1	24.42	88.8
{Zn(btmb)Cl ₂ } (4)	1.357	848.7	0.7554	103.0	46.7	89.4

Antimicrobial assays

The present method used to evaluate the antimicrobial activity of the prepared complexes was carried out by replacement the paper disc, used in standard method [72], with a solid tablet of the test compound adsorbed onto an adsorbing agent (peptone). This modification was introduced as a result of the low water solubility of the tested compounds which reduce their diffusion on the agar plate. The results of the antimicrobial screening of the prepared compounds are summarized in Table 7.

The comparison of inhibition zone diameters revealed that the majority of the tested complexes were found to have moderate to good antimicrobial activities against *Staphylococcus aureus*, *Pichia caribbica* and *Pseudomonas syringae* and are more efficient vs. this latter compared with the standard drug. However, in all case, no activity was observed against *Klebsiella pneumonia*.

Furthermore, in most case, the comparison of antimicrobial activities of the complexes with theirs corresponding ligands show that the presence of metal in the molecule skeleton increase the antibacterial activity against *Pseudomonas syringae*, *Staphylococcus aureus* and *Pichia caribbica*. However, the nature of metal or the ligand type doesn't have a significant effect in inhibition zone diameters.

Table 7

In Vitro Antibacterial activity of ligands bbms, btmb and complexes **1-4**.

	<i>Inhibition zones in mm</i>			
	<i>Ps</i>	<i>Sa</i>	<i>Kp</i>	<i>Pc</i>
{Co(bbms)Cl ₂ } (1)	16	27	0	25
{Zn(bbms)Cl ₂ } (2)	15	30	0	18
{Co(btmb)Cl ₂ } (3)	20	27	0	22
{Zn(btmb)Cl ₂ } (4)	22	15	0	0
Btmb	12	0	0	0
Bbms	12	0	0	0
benzylpenicilline sodique	0	50	0	6

Ps: Pseudomonas syringae; Sa: Staphylococcus aureus; Kp: Klebsiella pneumonia; Pc: Pichia caribbica.

Conclusion

In summary, four coordination metal complexes were synthesized by simple method. Single crystal X-Ray diffraction analysis of all complexes reveals their monomeric tetra-coordinated nature. The coordination polyhedron around the metal center may be described as a quasi-regular tetragonal geometry. The results of corrosion inhibition efficiency evaluation show that the prepared complexes can be effectively used as corrosion inhibitors for steel in acid medium. The order of the inhibition efficiency of the complexes as given by polarization measurements is in good agreement with that obtained from electrochemical impedance measurements. Potentiostatic polarization data indicated that these compounds are mixed-type inhibitors. In other hand, all complexes were evaluated for their in vitro antimicrobial activity against *Pseudomonas syringae*, *Staphylococcus aureus*, *Klebsiella pneumonia* and *Pichia caribbica*. In most cases, the prepared complexes have shown moderate to significant antimicrobial activities against *Staphylococcus aureus*, *Pichia caribbica* and *Pseudomonas syringae*. DFT/BP86 calculations carried out on neutral **1-4** complexes showed similarities between optimized models and experimental structures. Moreover, a careful analysis of their

electronic structures indicated almost identical characteristics of neutral Co(II) on one hand and the Zn(II) on other hand, but the reduced Co(I) forms behave differently in accordance with the $(\text{CH}_2)_n\text{S}$ bridge length and adopting different structures than those of the neutral ones and allowing a flexibility to the metal coordination sphere.

Acknowledgements

This work was supported by Mentouri Brothers University (Algeria). The authors thank MESRS and DGRST for financial support. A. Bouraiou thanks Dr. Sara Mahdjoub for his technical assistance in biological evaluation.

Appendix

Supplementary data CCDC 1432478–1432481 contains the supplementary crystallographic data for $\{\text{Co}(\text{bbms})\text{Cl}_2\}$, $\{\text{Co}(\text{btmb})\text{Cl}_2\}$, $\{\text{Zn}(\text{bbms})\text{Cl}_2\}$ and $\{\text{Zn}(\text{btmb})\text{Cl}_2\}$, respectively. These data can be obtained free of charge via <http://www.ccdc.cam.ac.uk/conts/retrieving.html>, or from the Cambridge Crystallographic Data Centre, 12 Union Road, Cambridge CB2 1EZ, UK; fax: (+44) 1223-336-033; or e-mail: deposit@ccdc.cam.ac.uk. Supplementary data associated with this article can be found, in the online version, at <http://dx.doi.org/10.1016/j.poly>.....

References

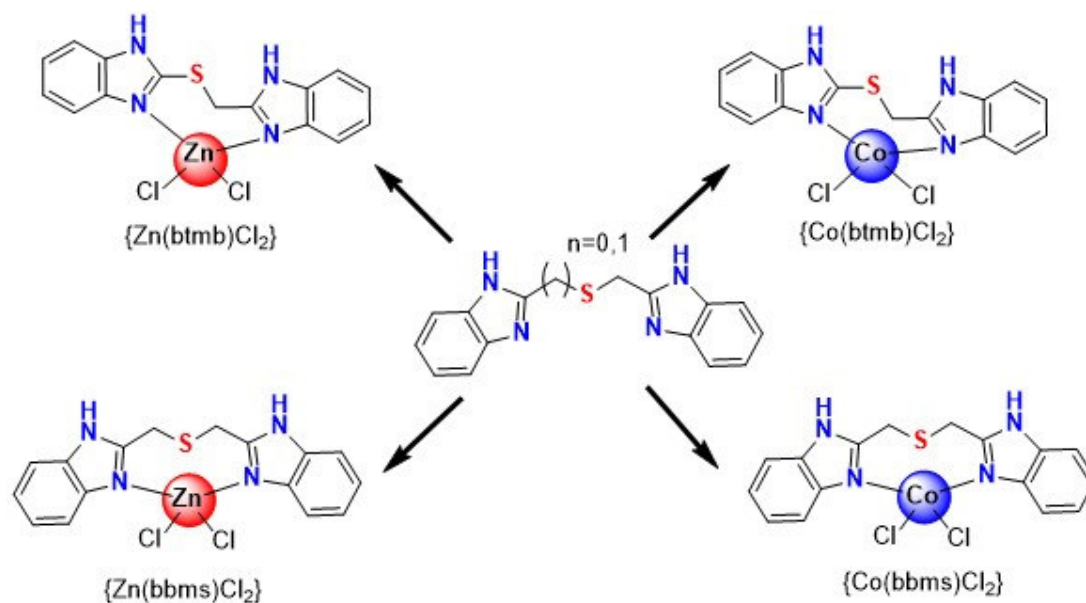
- [1] C. Kus, A. G. Kilcigil, B. C. Eke, M. Iscan, Arch. Pharm. Res. 27 (2004) 156.
- [2] P. N. Preston, Chem. Rev. 74 (1974) 279.
- [3] J. C. Hazelton, B. Iddon, H. Suschitzky, L. H. Woolley, Tetrahedron 51 (1995) 10771.
- [4] K. Paul, A. Sharma, V. Luxami, Bioorg. Med. Chem. Lett. 24 (2004) 624.
- [5] K. Vasantha, G. Basavarajaswamy, M. V. Rai, P. Boja, V. R. Pai, N. Shruthi, M. Bhat, Bioorg. Med. Chem. Lett. 25 (2015) 1420.
- [6] P. -J. Chen, A. Yang, Y. -F. Gu, X. -S. Zhang, K. -P. Shao, D. -Q. Xue, P. He, T. -F. Jiang, Q. -R. Zhang, H. -M. Liu, Bioorg. Med. Chem. Lett. 24 (2014) 2741.
- [7] K. F. Ansari, C. Lal, Eur. J. Med. Chem. 44 (2009) 4028.
- [8] Q. F. Li, R. H. He, J. O. Jensen, N. J. Bjerrum, Chem. Mater. 15 (2003) 4896.
- [9] Y. Abboud, A. Abourriche, T. Saffaj, M. Berrada, M. Charrouf, A. Bennamara, A. Cherqaoui, D. Takky, Appl. Surf. Sci. 252 (2006) 8178.
- [10] V. Z. Mota, G. S. de Carvalho, A. D. da Silva, L. A. Costa, P. de Almeida Machado, E. S. Coimbra, C. V. Ferreira, S. M. Shishido, A. Cuin, Biometals 27 (2014) 183.
- [11] F. Téllez, H. López-Sandoval, S. E. Castillo-Blum, N. Barba-Behrens, ARKIVOC v (2008) 245.

- [12] X. Qiao, Z. Y. Ma, J. Shao, W. G. Bao, J. Y. Xu, Z. Y. Qiang, J. S. Lou, *Biometals* 27 (2014) 155.
- [13] R. J. Sundberg, R. B. Martin, *Chem. Rev.* 74 (1974) 471.
- [14] J. Reedijk, In. «Comprehensive Coordination Chemistry»; G. Wilkinson, Ed.; Pergamon: Oxford, U. K., Vol. 2, Chap. 13 (1987).
- [15] M. Devereux, D. O'Shea, M. O'Connor, H. Grehan, G. Connor, M. McCann, G. Rosair, F. Lyng, A. Kellett, M. Walsh, D. Egan, B. Thati, *Polyhedron* 26 (2007) 4073.
- [16] M. Poyraz, M. Sari, F. Demirci, M. Kosar, S. Demirayak, O. Büyükgüngör, *Polyhedron* 27 (2008) 2091.
- [17] A. Kumar, A. Kumar, R. K. Gupta, R. P. Paitandi, K. B. Singh, S. K. Trigun, M. S. Hundal, D. S. Pandey, *J. Organomet. Chem.* 801 (2016) 68.
- [18] D. Zhang, Y. Tang, S. Qi, D. Dong, H. Cang, G. Lu, *Corros. Sci.* 102 (2016) 517.
- [19] M. Yadav, S. Kumar, T. Purkait, L. O. Olasunkanmi, I. Bahadur, E. E. Ebenso, *J. Mol. Liq.*, 213 (2016) 122.
- [20] A. Dutta, S. Kr. Saha, P. Banerjee, D. Sukul, *Corros. Sci.* 98 (2015) 541.
- [21] N. Benhamada, R. Bouchene, S. Bouacida, B. Zouchoune, *Polyhedron* 91 (2015) 59.
- [22] S. -M. Zendaoui, B. Zouchoune, *N. J. Chem.*, DOI: 10.1039/C5NJ02595H.
- [23] F. Zouchoune, S. -M. Zendaoui, N. Bouchakri, A. Djedouani, B. Zouchoune, *J. Mol. Struct.* 945 (2010) 78.
- [24] S. Farah, H. Korichi, S. -M. Zendaoui, J. Y. Saillard, B. Zouchoune, *Inorg. Chim. Acta.* 362 (2009) 3541.
- [25] S. Farah, N. Bouchakri, S. M. Zendaoui, J. Y. Saillard, B. Zouchoune, *J. Mol. Struct.* 953 (2010) 143.
- [26] A. Saiad, B. Zouchoune, *Can. J. Chem.* 93 (2015) 1096.
- [27] V. Klimešová, J. Kočí, M. Pour, J. Stachel, K. Waisser, J. Kaustová, *Eur. J. Med. Chem.* 37 (2002) 409.
- [28] N. M. Agh-Atabay, B. Dulger, F. Gucin, *Eur. J. Med. Chem.* 38 (2003) 875.
- [29] P. Kopel, D. Wawrzak, V. Langer, K. Cihalova, D. Chudobova, R. Vesely, V. Adam, R. Kizek, *Molecules* 18 (2013) 11978.
- [30] M. C. Burla, R. Caliendo, M. Camalli, B. Carrozzini, G.L. Cascarano, L. De Caro, C. Giacobazzo, G. Polidori, R. Spagna, *J. Appl. Cryst.* 38 (2003) 381.
- [31] G. M. Sheldrick, *Acta Cryst. A* 64 (2008) 112.
- [32] L. J. Farrugia, *J. Appl. Cryst.* 45 (2012) 849.
- [33] G. M. Sheldrick, SADABS Bruker AXS Inc., Madison, Wisconsin, USA (2002).

- [34] K. Brandenburg, M. Berndt, (2001). DIAMOND. Crystal Impact, Bonn, Germany.
- [35] L. J. Farrugia, *J. Appl. Cryst.* 30 (1997) 565.
- [36] ADF2013.01, Theoretical Chemistry, Vrije Universiteit: Amsterdam, The Netherlands, SCM.
- [37] E. J. Baerends, D. E. Ellis, P. Ros, *Chem. Phys.* 2 (1973) 41.
- [38] G. te Velde, E. J. Baerends, *J. Comput. Phys.* 99 (1992) 84.
- [39] C. Fonseca Guerra, J. G. Snijders, G. te Velde, E. J. Baerends, *Theo. Chim. Acc.* 99 (1998) 391.
- [40] F. M. Bickelhaupt, E. J. Baerends, *Rev. Comput. Chem.* 15 (2000) 1.
- [41] G. te Velde, F. M. Bickelhaupt, C. Fonseca Guerra, S. J. A. van Gisbergen, E. J. Baerends, J.G. Snijders, T. Ziegler, *J. Comput. Chem.* 22 (2001) 931.
- [42] S. D. Vosko, L. Wilk, M. Nusair, *Can. J. Chem.* 58 (1990) 1200.
- [43] A. D. Becke, *J. Chem. Phys.* 84 (1986) 4524.
- [44] A. D. Becke, *Phys. Rev. A.* 38 (1988) 3098.
- [45] J. P. Perdew, *Phys. Rev. B.* 33 (1986) 8822.
- [46] J. P. Perdew, *Phys. Rev. B.* 34 (1986) 7406.
- [47] L. Versluis, T. Ziegler, *J. Chem. Phys.* 88 (1988) 322.
- [48] L. Fan, T. Ziegler, *J. Chem. Phys.* 96 (1992) 9005.
- [49] L. Fan, T. Ziegler, *J. Phys. Chem.* 96 (1992) 6937.
- [50] N. M. Agh-Atabay, B. Dulger, F. Gucin, *Eur. J. Med. Chem.* 40 (2005) 1096.
- [51] T. Pandiyan, J. Guadalupe Hernández, N. Trejo Medina, S. Bernés, *Inorg. Chim. Acta* 357 (2004) 2570.
- [52] W. Clegg, J. C. Lockhart, F. H. Musa, *J. Chem. Soc., Dalton Trans.* (1986) 47.
- [53] R. Cariou, J. J. Chirinos, V. C. Gibson, G. Jacobsen, A. K. Tomov, G. J. P. Britovsek, A. J. P. White, *Dalton Trans.* 39 (2010) 9039.
- [54] L. Mishra, A.K. Pandey, U.C. Agarwala, *Indian J. Chem., Sect. A* 32 (1993) 442.
- [55] R. Gregorzik, H. Vahrenkamp, *Chem. Ber.* 127 (1994) 1857.
- [56] C. J. Matthews, W. Clegg, S. L. Heath, N. C. Martin, M. N. S. Hill, J. C. Lockhart, *Inorg. Chem.* 37 (1998) 199.
- [57] K. Ogawa, K. Nakata, K. Ichikawa, *Bull. Chem. Soc. Jpn.* 70 (1997) 2925.
- [58] J. Bernstein, R.E. Davis, L. Shimoni, N.-L. Chang, *Angew. Chem. Int. Ed. Engl.* 34 (1995) 1555.
- [59] M. C. Etter, J. C. MacDonald, J. Bernstein, *Acta Cryst. B*46 (1990) 256.

- [60] A. K. Satapathy, G. Gunasekaran, S. C. Sahoo, K. Amit, P. V. Rodrigues, *Corros. Sci.* 51 (2009) 2848.
- [61] Y. Yan, W. H. Li, L. K. Cai, B. R. Hou, *Electrochim. Acta* 53 (2008) 5953.
- [62] M. Farsak, H. Keleş, M. Keleş, *Corros. Sci.* 98 (2015) 223.
- [63] M. Mahdavian, A. M. M. Attar, *Electrochim. Acta* 50 (2005) 4645.
- [64] F. Mansfeld, M. W. Kendig, S. Tsai, *Corrosion* 38 (1982) 478.
- [65] J. R. Macdonald, *Impedance Spectroscopy*, John Wiley & Sons, New York (1987).
- [66] L. -G. Qiu, A. -J. Xie, Y. -H. Shen, *Mat. Chem. Phys.* 91 (2005) 269.
- [67] A. Ghanbari, M.M. Attar, M. Mahdavian, *Mat. Chem. Phys.* 124 (2010) 1205.
- [68] J. Cruz, T. Pandiyan, E. Garcia-Ochoa, *J. Electroanal. Chem.* 583 (2005) 8.
- [69] S. Şafak, B. Duran, A. Yurt, G. Türkoğlu, *Corros. Sci.* 54 (2012) 251.
- [70] N. Dinodi, A. N. Shetty, *Corros. Sci.* 85 (2014) 411.
- [71] M. A. Hegazy, *J. Mol. Liq.* 208 (2015) 227.
- [72] P. Couvalin, R. Leclerc, E. Bingen, *Antibiogramme*, 2nd ed.; Eds. ESKA, France, (1985).

Graphical abstract



Synopsis

Synthesis, characterization and DFT analysis of $\{Co(bbms)Cl_2\}$, $\{Zn(bbms)Cl_2\}$, $\{Co(btmb)Cl_2\}$ and $\{Zn(btmb)Cl_2\}$ containing benzimidazole thioether have been described. These later show the corrosion inhibition ability of the prepared complexes for steel in acid medium. Furthermore, these complexes show moderate to significant antimicrobial activities. DFT/BP86 calculations have been carried out.